Acta Biochim Biophys Sin xxxx, xx(x): xx-xx
https://cstr.cn/32197.14.abbs.2026053
https://doi.org/10.3724/abbs.2026053
Original Article

Original Article

The macrophage PELI1-JAK2/STAT3-secretome axis: a potential target for ameliorating septic inflammation and coagulation dysfunction

Yi Huang†, Lizhen Xuan†, Kunlin Zhou†, Linli Wang†, Yiran He, Xu Wang, Mingchen Han, Shengyu Hao*, and Minjie Ju*

Department of Critical Care Medicine, Zhongshan Hospital, Fudan University, Shanghai 200032, China
†These authors contributed equally to this work.
*Correspondence address. E-mail: janet9yu@163.com (S.H.); ju.minjie@zs-hospital.sh.cn (M.J.)

Received 08 November 2025 Accepted 9 January 2026 Published 23 June 2026

Abstract

This study aims to investigate the role of macrophage PELI1 in sepsis-induced inflammation and coagulation dysfunction, focusing on its regulatory mechanism over the secretome through the JAK2/STAT3 signaling pathway. Analysis of a public single-cell RNA-seq dataset from septic patients reveals significant upregulation of PELI1 in $CD14^+$ monocytes from non-survivors. To functionally validate this finding, a murine sepsis model is established using cecal ligation and puncture (CLP). Protein and gene expression levels in lung tissue and plasma are detected by RT-qPCR, western blotting, and ELISA, while lung injury and fibrin deposition are assessed by H&E staining and immunohistochemistry. For *in vitro* experiments, PELI1 expression is modulated in RAW264.7 macrophages using gene knockdown strategies. Our results confirm that PELI1 is significantly upregulated in septic mice and closely associates with severe inflammatory responses and coagulation dysfunction. Mechanistically, *PELI1* knockout suppresses the activation of the JAK2/STAT3 signaling pathway, thereby reducing the production and secretion of key inflammatory cytokines and coagulation factors induced by lipopolysaccharide. Importantly, transfer of the secretome from bone marrow-derived macrophages (BMDM) of *PELI1*-knockout mice into wild-type septic mice is sufficient to alleviate sepsis pathology, which recapitulates the protective effect observed in genetic knockout. Our findings demonstrate that PELI1 mediates sepsis-induced tissue injury by regulating the secretome via the JAK2/STAT3 pathway, which identifies the PELI1-secretome axis as a potential therapeutic target for this life-threatening condition.

Key words PELI1, macrophage, sepsis, coagulation dysfunction, JAK2/STAT3 signaling pathway

Introduction

Sepsis is a life-threatening organ dysfunction caused by a dysregulated host response to infection [1,2], contributing to over eleven million annual deaths globally [3]. Its core pathophysiology involves dysregulated inflammation and coagulation [4,5]. However, the precise molecular connectors that integrate these two processes remain unclear, impeding the development of targeted therapies.

Macrophages are central players in the pathogenesis of sepsis, driving critical processes in acute lung injury, inflammation, and coagulation [6,7]. Research has demonstrated that changes in macrophage functional status shape their secretome profile [8,9]. During the early stages of sepsis, activated macrophages undergo functional reprogramming, leading to a profound shift in secretion. On the one hand, these cells release large quantities of pro-inflammatory cytokines such as IL-1, IL-6, and TNF-α [4,5]; on the other hand, the expression and secretion of macrophage-derived procoagulant factors, most notably tissue factor (TF, a direct initiator of coagulation) and plasminogen activator inhibitor-1 (PAI-1, a key fibrinolysis inhibitor potently upregulated by macrophage cytokines), are enhanced [10–15]. While the individual roles of specific inflammatory and procoagulant factors in sepsis have been

© The Author(s) 2026. This is an open access article distributed under the terms of the Creative Commons Attribution License (https://creativecommons.org/licenses/by/4.0/).

extensively studied, the upstream regulators that enable the macrophage secretome to orchestrate both inflammatory and coagulant responses in sepsis are poorly understood. Identifying such regulators could provide new mechanistic insights into septic coagulation dysfunction. Herein, we focused on TF and PAI-1 as canonical effectors to dissect this regulatory axis.

PELI1, an E3 ubiquitin ligase, is a key component of TLR signaling in myeloid cells [16] and regulates inflammatory responses and macrophage polarization [17,18]. Recent studies have unveiled a significant role of PELI1 in activating pattern recognition receptors (PRR) such as Toll-like receptors (TLR), T-cell receptors, and cytokine receptors, to mediate inflammation and autoimmunity. Recent evidence has expanded its relevance to sepsis, showing that DAPK-mediated destabilization of this protein exacerbates renal inflammatory injury [19]. A key mechanistic insight comes from studies demonstrating that PELI1 regulates the ubiquitination and degradation of the transcription factor STAT3, playing a pivotal role in inflammation and inflammation-related cancer development and thereby positioning STAT3 as a critical downstream mediator [20]. Building on this established link between PELI1 and STAT3 regulation and given the known role of the JAK-STAT pathway in controlling procoagulant factors in macrophages [21,22], we hypothesized that PELI1 contributes to coagulation dysfunction in sepsis by modulating JAK2/STAT3 pathway activity.

In this study, we established a *PELI1*-deficient cell line to investigate the role of macrophage PELI1 in the development of inflammation and coagulation dysfunction in sepsis. *PELI1* knockdown reduced LPS-induced expression of inflammatory and coagulation-related factors, thereby inhibiting the progression of septic coagulation dysfunction. Specifically, PELI1 promoted septic inflammation and coagulation dysfunction by driving pathologic reprogramming of the macrophage secretome through JAK2/STAT3 signaling. Our findings reveal that macrophage PELI1 plays an important role in macrophage function, affecting the development of septic inflammation and coagulation dysfunction.

Materials and Methods

Data selection and single-cell RNA sequencing data processing

We analyzed the GEO dataset GSE167363 (https://www.ncbi.nlm.nih.gov/geo/), comprising peripheral blood mononuclear cells (PBMCs) samples from five sepsis patients (two nonsurvivors and three survivors). Data processing and analysis were performed using Seurat (v 4.3.0). Quality control was applied as follows: genes expressed in fewer than three cells and cells expressing fewer than 200 or more than 6500 genes were excluded. Additionally, cells were filtered to keep only those with less than 25% of transcripts mapping to mitochondrial genes (Supplementary Figure S1A). Data were normalized using the NormalizeData function, and the top 2000 highly variable genes were selected. The Harmony algorithm (v 1.2.3) was used for correcting batch effects among samples. The first 50 principal components, determined from the PCA elbow plot (Supplementary Figure S1B), were used for downstream analyses. Cell clustering was performed using the FindClusters function with resolution set to 0.5, and the results were visualized by UMAP (Supplementary Figure S1C,D). Cell types were annotated based on canonical marker gene expression patterns (Supplementary Figure S1E–G), which identified $CD4^+$ T cells, $CD8^+$ T cells, Tregs, $CD14^+$/$CD16^+$ monocytes, B cells, plasmablasts, and platelets. Differential gene expression analysis was conducted using the FindMarkers function (Wilcoxon rank sum test) with an adjusted P value < 0.05 and $|\text{avg_log}_2\text{FC}| \geq 0.25$. This analysis indicated that PELI1 was upregulated in $CD14^+$ (expression rate: NS 62% vs S 35%; $\log_2\text{FC} = 0.87$, adjusted P-value $= 2.14 \times 10^{-144}$) monocytes from non-survivors. Cells were classified as $PELI1^+$ or $PELI1^-$ based on PELI1 expression, which confirmed that its expression differences were highest and most specific in monocytes. All analyses were performed in R (v 4.2.0) with the packages tidyverse and patchwork. Visualizations were generated using ggplot2 or the built-in Seurat functions.

Clinical sample analysis

This study was approved by the Ethics Committee of Zhongshan Hospital, Fudan University (approval No. B2023-074R) and conducted in accordance with the principles of the Declaration of Helsinki. Peripheral blood samples were collected from septic patients (survivors and non-survivors) with informed consent.

Isolation and flow cytometric sorting of human $CD14^+$ monocytes

$CD14^+$ monocytes were isolated from human venous blood. PBMCs were first separated by density gradient centrifugation: 10 mL of EDTA-anticoagulated whole blood was diluted 1:1 with PBS, layered over 10 mL of Lymphocyte Separation Medium (Dakewe, Shenzhen, China), and centrifuged at 800 *g* for 20 min (18°C). The PBMC layer was collected, washed with PBS, and centrifuged at 400 *g* for 5 min (4°C). For sorting, PBMCs were resuspended in 200 μL of PBS, stained with 5 μL of PE-conjugated anti-human CD14 antibody (PE-65056; Proteintech, Wuhan, China) for 20 min at 4°C in the dark, washed, and then incubated with 5 μL of 7-aminoactinomycin D (7-AAD, 17501; AAT Bioquest, Sunnyvale, USA) in 1 mL of PBS for 10 min to label dead cells. Viable $CD14^+$ monocytes were purified using a BD FACSAria III sorter (BD Life Sciences, Milpitas, USA). The sorted cells were immediately processed for subsequent protein and RNA analysis.

Animal details

Male C57BL/6J mice (8 weeks old) were obtained from Shanghai SLAC Laboratory Animal Co., Ltd. (Shanghai, China). Mice were housed under specific pathogen-free conditions at 23 ± 3°C and 55 ± 10% relative humidity with a 12-h light/dark cycle and provided food and water ad libitum. *PELI1*-knockout mice were generated and provided by the laboratory of Professor Jinsong Li at the Center for Excellence in Molecular Cell Science, Chinese Academy of Sciences (Shanghai, China). The study was approved by the Ethics Committee of Zhongshan Hospital, Fudan University (approval No. 2025-193).

Cecal ligation and puncture (CLP) model

Mice were anesthetized with 1% sodium pentobarbital (Solarbio, Beijing, China) at a dose of 100 μL per 10 g body weight. A midline abdominal incision was made to expose the cecum. The distal portion was ligated with 4-0 silk suture and punctured twice using a 21-gauge needle (Kindly, Shanghai, China). A small quantity of fecal content was gently extruded before returning the cecum to the abdominal cavity. The abdominal wall was closed in layers. Sham-operated mice underwent the same surgical procedure excluding ligation and puncture. Postoperatively, all mice received 1 mL of

pre-warmed saline subcutaneously for fluid resuscitation. After 24 h, lung tissues were collected and either fixed in 4% paraformaldehyde for histological analysis or snap-frozen and stored at −80°C for molecular analyses. Whole blood samples were centrifuged at 1500 *g* for 15 min to isolate plasma, which was aliquoted and stored at −80°C.

Plasma separation

At 24 h post-CLP, the mice were deeply anesthetized with 1% sodium pentobarbital. Approximately 0.5–1.0 mL of whole blood was collected via cardiac puncture using K_2EDTA anticoagulant tubes (365974; BD Microtainer, Franklin Lakes, USA). Tubes were gently inverted several times and centrifuged at 1500 *g* for 15 min at 4°C. The supernatant (plasma) was carefully collected, snap-frozen in liquid nitrogen, and stored at −80°C for subsequent assays.

Generation of bone marrow-derived macrophages (BMDMs)

Mice were euthanized in a CO_2 chamber, and death was confirmed by cervical dislocation. Femurs and tibias were harvested from C57BL/6J mice. Bone marrow cells were isolated, treated with red blood cell lysis buffer (Solarbio), and resuspended in complete DMEM (11965092; Gibco, Waltham, USA) supplemented with 10% fetal bovine serum (FBS, A5256701; Gibco), 1% penicillinstreptomycin (15140122; Gibco), and 20 ng/mL recombinant mouse M-CSF (Z02930; GenScript, Nanjing, China). On day 3, half of the medium was replaced with fresh medium containing M-CSF. By day 7, the adherent cells, which exhibited typical macrophage morphology under an inverted light microscope (DMi1; Leica Microsystems, Wetzlar, Germany), were harvested as bone marrow-derived macrophages (BMDMs) for subsequent experiments.

RNA isolation and quantitative real-time PCR (qPCR)

Total RNA was extracted from lung tissues or cells using the MolPure Cell/Tissue Total RNA Kit (19221ES60; Yeasen, Shanghai, China). A total of 1000 ng RNA was reverse-transcribed into cDNA using All-In-One 5× RT MasterMix (BL1020A; Biosharp, Hefei, China). qPCR was performed using SYBR Green reagent (A57156; Thermo Fisher Scientific, Waltham, USA) on a CFX Opus 96 system (Bio-Rad, Hercules, USA). *GAPDH* served as the internal reference. Relative mRNA expression was calculated using the $2^{-\Delta\Delta Ct}$ method, with all fold changes normalized to the untreated control. Primer sequences are provided in Supplementary Table S1.

Enzyme-linked immunosorbent assay (ELISA)

Commercial ELISA kits for thrombin-antithrombin complex (TAT, E-EL-M1138m; Elabscience, Wuhan, China), D-dimer (E-EL-M0400m; Elabscience), tissue factor (TF, E-EL-M1163m; Elabscience), plasminogen activator inhibitor-1 (PAI-1, E-MSEL-M0098m; Elabscience), TNF-α (DY410m; R&D Systems, Minneapolis, USA), IL-1β (DY401m; R&D Systems), and IL-6 (DY406m; R&D Systems) were used to measure their concentrations in mouse plasma or macrophage culture supernatant according to the manufacturers' instructions. Briefly, samples and standards were added to ELISA plates pre-coated with specific antibodies and incubated at room temperature. After washing, detection antibodies and enzyme conjugates were added sequentially, followed by substrate solution. The reaction was stopped with stop solution, and absorbance was measured at 450 nm using a microplate reader (Synergy HTX; BioTek Instruments, Winooski, USA).

Western blotting

Total protein was extracted from lung tissues or RAW264.7 cells using RIPA buffer (539134; Millipore, Burlington, USA) containing protease and phosphatase inhibitors (20109; Yeasen). The protein concentration was determined by BCA assay (Biosharp). Equal amounts of protein were separated by 10% SDS-PAGE and transferred to nitrocellulose membranes (IPVH85R; Millipore). After blocking with 5% skim milk, membranes were incubated overnight at 4°C with primary antibodies against PELI1 (31474, 1:1000; Cell Signaling Technology, Danvers, USA; or 12053-1-AP, 1:500; Proteintech), TF (83887-4-RR, 1:2000; Proteintech), PAI-1 (66261-1-Ig, 1:2000; Proteintech), p-STAT3 (9145, 1:1000; Cell Signaling Technology), STAT3 (9139, 1:1000; Cell Signaling Technology), p-JAK2 (3776, 1:1000; Cell Signaling Technology), JAK2 (3230, 1:1000; Cell Signaling Technology), β-actin (66009-1-Ig, 1:2000; Proteintech), β-tubulin (66240-1-Ig, 1:2000; Proteintech), HRP-conjugated Goat Anti-Rabbit IgG (7074, 1:2000; Cell Signaling Technology), HRP-conjugated Horse Anti-Mouse IgG (7076, 1:2000; Cell Signaling Technology). The membranes were washed and incubated with HRP-conjugated secondary antibodies for 1 h at room temperature, and protein signals were detected using enhanced chemiluminescence. Quantification was performed using ImageJ (version 1.54g; NIH, Bethesda, USA).

In vivo supernatant reconstitution assay in mice

BMDMs were isolated from three wild-type (WT) and three *Peli1*$^{-/-}$ mice as described above. Cells were seeded at 1×10^6 cells per well in 6-well plates. After 12 h of adherence, the medium was replaced with serum-free DMEM for 2 h, followed by stimulation with 100 ng/mL LPS (*E. coli* O55:B5; Sigma, St Louis, USA) in serum-free DMEM for 6 h. Supernatants were collected, centrifuged at 2000 *g* for 20 min at 4°C, and stored as conditioned medium (CM) at −80°C. CM from three WT or three *Peli1*$^{-/-}$ mice was pooled to create WT CM and KO CM pools, respectively. Pooled CM was filtered through 0.22-μm low protein-binding filters. Protein concentrations were measured by BCA assay, and WT CM was adjusted to match the KO CM concentration (15 μg/mL) using serum-free DMEM. Immediately after CLP surgery, mice received an intraperitoneal injection of 100 μL adjusted WT CM (WTsup + CLP group) or KO CM (KOsup + CLP group). The control, CLP, and KO + CLP groups received an equal volume of serum-free medium. Blood and lung tissues were collected 24 h post-injection for analysis.

Histopathological analysis and immunohistochemistry

Mice were euthanized, and lung tissues were collected, fixed in 4% paraformaldehyde, dehydrated, paraffin-embedded, sectioned, and deparaffinized. Sections were stained with hematoxylin and eosin (H&E) for histological evaluation. For immunohistochemistry, antigen retrieval was performed by heating in citrate buffer. After blocking with 1% bovine serum albumin (Sigma, B2064), the sections were incubated overnight at 4°C with primary antibodies against PELI1 (1:50; Proteintech), F4/80 (1:100; Servicebio, Wuhan, China), and fibrin(ogen) (1:100; Servicebio). This was followed by incubation with HRP-conjugated goat anti-rabbit secondary antibody, DAB staining, and hematoxylin counterstaining. The expression of PELI1, F4/80, and fibrin(ogen) was imaged under a light microscope.

Immunofluorescence staining

Lung tissue sections from septic mice were deparaffinized, rehydrated, and subjected to antigen retrieval. After blocking, the sections were incubated overnight at 4°C with primary antibodies against PELI1 and F4/80. Subsequently, appropriate fluorescent secondary antibodies were applied in the dark at room temperature for 1 h. The nuclei were counterstained with DAPI. Images were captured using a fluorescence microscope.

Cell culture

The murine macrophage cell line RAW264.7 (ATCC, Manassas, USA) was cultured in DMEM supplemented with 10% FBS and 1% penicillinstreptomycin at 37°C in a 5% CO_2 incubator. Cells within 10 passages were used. RAW264.7 cells were seeded in 6-well or 12-well plates and cultured overnight until 60%–70% confluence and then stimulated with 100 ng/mL LPS for 6 h.

Construction of lentivirus-mediated *PELI1* stable knockdown cell line

A *PELI1*-knockdown RAW264.7 cell line was generated using lentiviral vector-mediated RNAi. The shRNA targeting mouse *Peli1* (5′-CGGTCAACTGAAAGTCCTATT-3′) and a non-targeting control (NTC; 5′-GCGCGATAGCGCTAATAATTT-3′) were constructed by Shanghai GeneChem (Shanghai, China). RAW264.7 cells were seeded at 5×10^4 cells/well in 6-well plates. After 24 h, lentiviral particles (MOI = 50) and 5 μg/mL polybrene (Sigma) were added. The medium was replaced 24 h post-infection. After 72 h, cells were selected with 5 μg/mL puromycin for 1–2 weeks until all control cells died. Knockdown efficiency was confirmed by western blotting and/or qPCR.

RNA sequencing

The shNC-RAW264.7 and shPELI1-RAW264.7 cells were plated at equal densities in T25 flasks and cultured at 37°C with 5% CO_2 until they reached 70% confluency. The medium was aspirated, and the cells were washed with PBS before lysis with 1 mL of TRIzol reagent (Invitrogen, Waltham, USA). The lysate was mixed thoroughly by pipetting, transferred to RNase-free tubes, snap-frozen in liquid nitrogen, and stored at −80°C. Samples were submitted to Sangon Biotech (Shanghai, China) for RNA extraction, quality control, library preparation, and sequencing. This experiment served as a preliminary, hypothesis-driven screening.

Statistical analysis

Statistical analyses were conducted using GraphPad Prism 9.0.0 (GraphPad Software, La Jolla, USA) and R v4.2.0. Each experiment was independently repeated at least three times. Data are expressed as the mean ± standard deviation (SD). Sample sizes (n) are indicated in the figure legends. Data normality and homogeneity of variances were assessed using the Shapiro-Wilk and Levene's tests, respectively. Depending on these results, comparisons between two groups were conducted using unpaired Student's t-tests (or Welch's t-tests when variances were unequal). For comparisons among multiple groups, one-way ANOVA followed by Tukey's *post hoc* test was performed when both assumptions were met; Brown-Forsythe ANOVA with the Games-Howell post hoc test was applied for normally distributed data with unequal variances; and the Kruskal-Wallis test followed by Dunn's *post hoc* test was used for non-normally distributed data. A P value less than 0.05 was considered statistically significant.

Results

PELI1 expression is elevated in CD14⁺ monocytes from non-survivors compared to survivors

We first analyzed single-cell transcriptomic data from the peripheral blood of sepsis survivors (S) and non-survivors (NS). UMAP dimensionality reduction and clustering systematically delineated the immune cell landscape, annotating ten major immune cell populations (Figure 1A and Supplementary Table S2). Comparative analysis revealed distinct overall immune cell compositions between the two groups (Figure 1B). Focusing on PELI1, we observed a clear spatial separation between PELI1⁺ and PELI1⁻ cells across multiple immune populations (Figure 1C). Further analysis demonstrated the specific enrichment of PELI1 in CD14⁺ monocytes from the NS group: UMAP feature plots showed a strong PELI1 signal within this cluster in NS, which was markedly weaker in S (Figure 1D). This qualitative finding was robustly supported by quantitative data; a dot plot confirmed that CD14⁺ monocytes from NS exhibited higher average PELI1 expression levels and a greater proportion of expressing cells than those from S (expression rate: NS 62% vs S 35%; $\log_2$FC = 0.87, adjusted $P = 2.14 \times 10^{-144}$) (Figure 1E).

To functionally validate these findings at both the transcriptional and protein levels, we isolated CD14⁺ monocytes from a separate cohort of septic patients using fluorescence-activated cell sorting (FACS) (gating strategy shown in Supplementary Figure S2). Consistent with the bioinformatic analysis, qPCR revealed that PELI1 mRNA expression was significantly higher in CD14⁺ monocytes from non-survivors than in those from survivors (Figure 1F). Critically, western blot analysis directly confirmed this upregulation at the protein level, showing markedly increased PELI1 protein abundance in monocytes from non-survivors (Figure 1G,H). Together, these results provide direct experimental evidence that PELI1 is elevated in CD14⁺ monocytes of septic non-survivors, strengthening the clinical relevance of our initial observation.

PELI1 upregulation exacerbates lung injury and coagulation dysfunction in murine sepsis

To establish the causal role of PELI1, we employed a murine sepsis model. In septic mice, the mRNA expression of PELI1 was increased in lung tissues compared with controls (Figure 2A). Meanwhile, the mRNA levels of coagulation-related factors TF and PAI-1 were markedly elevated (Figure 2B,C). Inflammatory mediators, including TNF-α, IL-6, and IL-1β, were also upregulated in septic lungs (Figure 2D–F). Consistent with these findings, plasma levels of coagulation markers, including D-dimer, TF, and TAT complex, were increased in septic mice (Figure 2G–I). Histopathological and immunohistochemical analyses revealed pronounced lung injury characterized by alveolar edema, fibrin deposition, and enhanced macrophage infiltration, all of which correlated strongly with PELI1 upregulation (Figure 2J). Western blot analysis further confirmed the elevated protein expression of PELI1, TF, and PAI-1 in septic lung tissues (Figure 2K–N). These findings link PELI1 expression with sepsis-induced lung injury and coagulation dysfunction.

PELI1 regulates macrophage inflammatory and procoagulant responses via JAK2/STAT3 signaling

To investigate how PELI1 regulates macrophage function, we generated a stable *PELI1*-knockdown RAW264.7 cell line (shPELI1) with a non-targeting control (shNC). The knockdown efficiency was validated by a significant reduction in both PELI1 mRNA (Figure 3A)

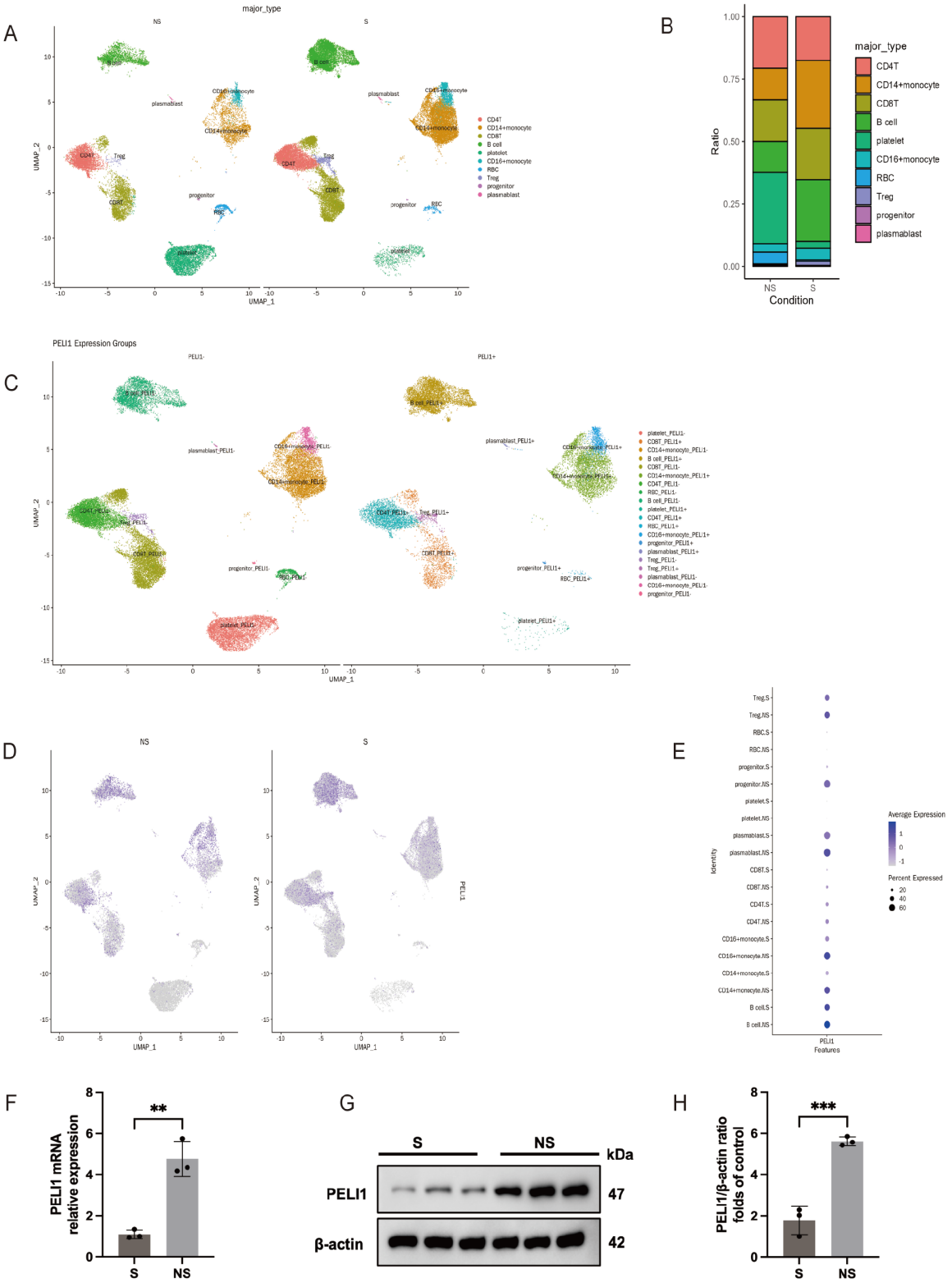


Figure 1. PELI1 is highly expressed in CD14⁺ monocytes of non-survivors (A) UMAP visualization of single-cell transcriptomic data from S and NS PBMCs. (B) Stacked bar chart displaying the proportional distribution of immune cell types in the S and NS groups. (C) UMAP plot showing the spatial distribution of PELI1⁺ (red) and PELI1⁻ (gray) cells across immune populations. (D) UMAP feature plots of PELI1 expression in the NS (left) and S (right) groups. (E) Dot plot showing the average expression level (color intensity) and percentage of PELI1-expressing cells (dot size) across different immune cell types. (F) *PELI1* mRNA levels in fluorescence-activated cell sorting (FACS)-isolated CD14⁺ monocytes from a validation cohort of septic patients (S vs. NS). (G, H) PELI1 protein levels from the same patient cohort. Data are presented as the mean ± SD ($n = 3$ patients per group), $^{**}P < 0.01$ and $^{***}P < 0.001$.

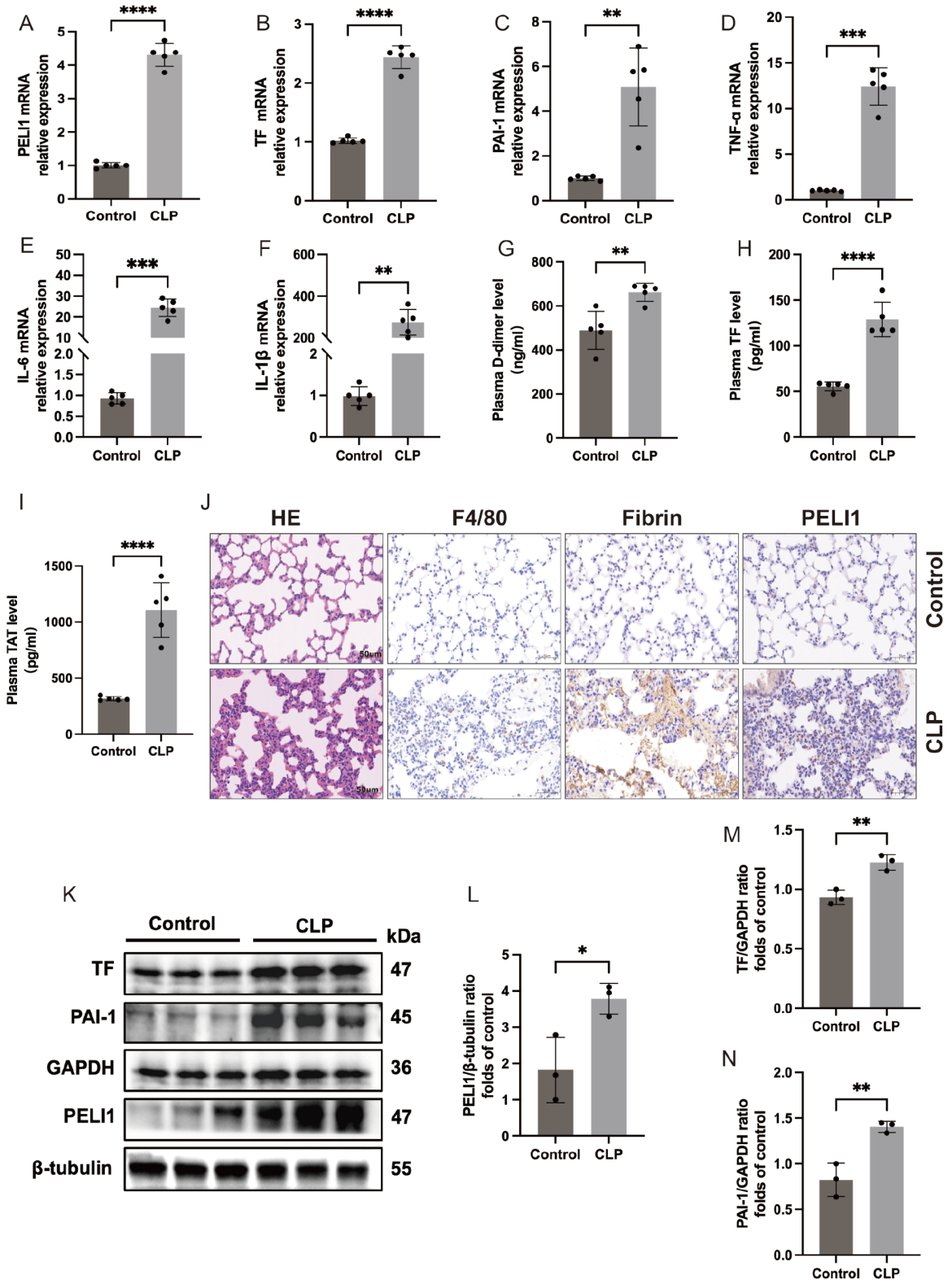


Figure 2. High PELI1 expression is associated with acute lung injury and coagulation activation in septic mice (A–F) Relative mRNA levels in murine lung tissues: (A) PELI1, (B) TF, (C) PAI-1, (D) TNF-α, (E) IL-6 , and IL-1β (F) ($n = 5$ mice per group). (G–I) Plasma levels of coagulation markers measured by ELISA: (G) D-dimer, (H) TF, and (I) TAT complex ($n = 5$ mice per group). (J) Representative images of lung sections subjected to H&E staining and immunohistochemical analysis for F4/80, fibrin, and PELI1 (scale bar: 50 μm). (K) Representative western blot images showing PELI1, TF, and PAI-1 protein expression in murine lung tissues. (L–N) Corresponding densitometric analyses of (L) PELI1, (M) TF, and (N) PAI-1 in murine lung tissues ($n = 3$ mice per group). Data are presented as the mean ± SD. $^{*}P < 0.05$, $^{**}P < 0.01$, $^{***}P < 0.001$, and $^{****}P < 0.0001$.

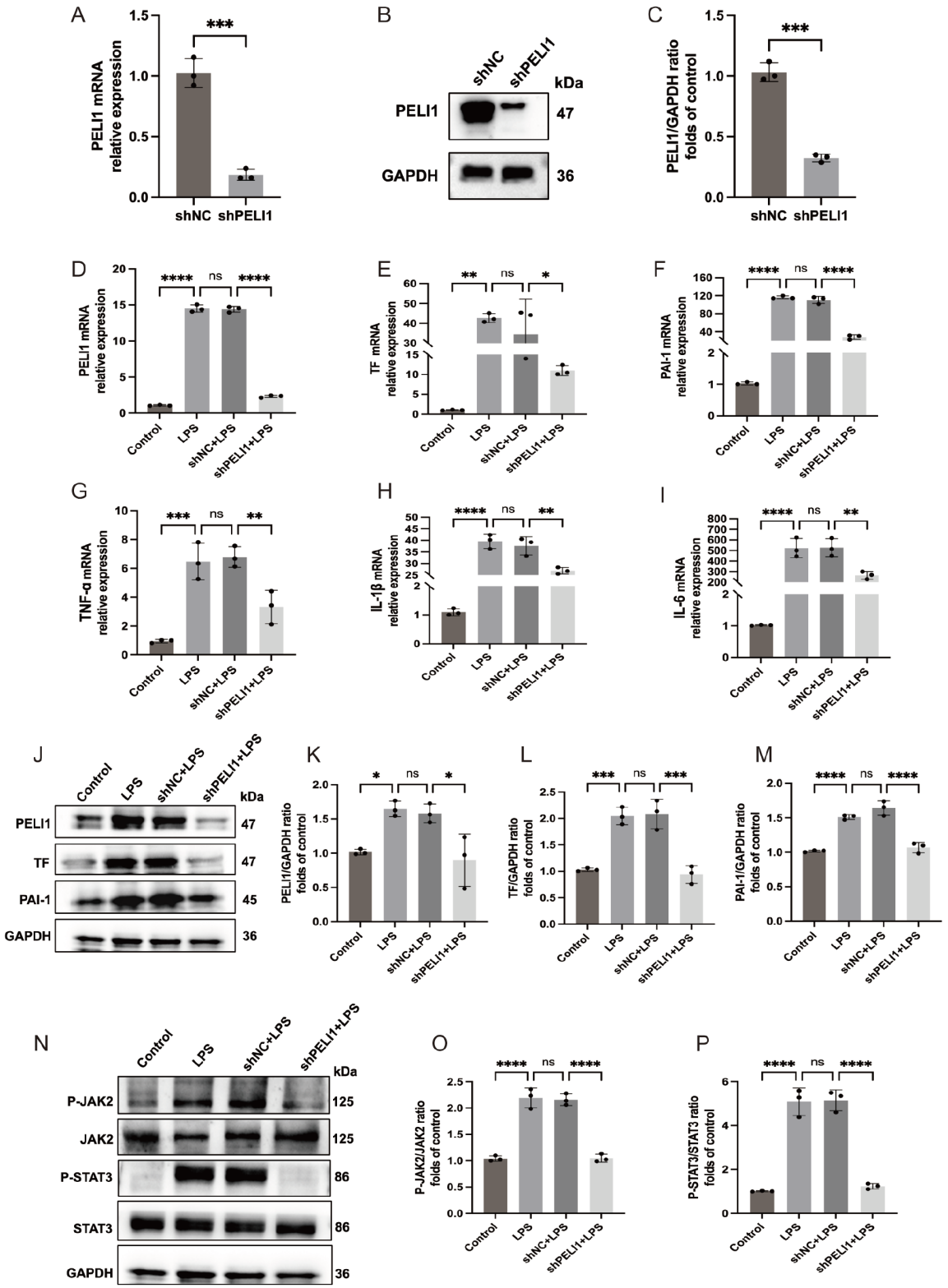


Figure 3. Knockdown of *PELI1* suppresses LPS-induced expression of inflammation and coagulation-related factors via the JAK2/STAT3 pathway (A) *PELI1* mRNA expression in RAW264.7 cells transfected with shNC or shPELI1. (B) Representative western blot images and (C) corresponding densitometric analysis of PELI1 protein expression. (D–I) mRNA expression of (D) PELI1, (E) TF, (F) PAI-1, (G) TNF-α, (H) IL-1β, and (I) IL-6 in shNC- or shPELI1-transfected RAW264.7 cells stimulated with LPS. (J–M) Representative western blot images and corresponding densitometric analyses of (K) PELI1, (L) TF, and (M) PAI-1. (N–P) Representative western blot images and corresponding densitometric analyses of (O) p-JAK2 and (P) p-STAT3. Data are presented as the mean ± SD. Data are representative of three independent experiments. *$P < 0.05$, **$P < 0.01$, *** $P < 0.001$, ****$P < 0.0001$, and ns, $P > 0.05$.

and protein levels (Figure 3B,C) under basal conditions. RNA sequencing under baseline conditions suggested involvement of the JAK-STAT pathway. To evaluate the functional consequences of *PELI1* knockdown under inflammatory conditions, cells were stimulated with LPS. Compared with control cells, shPELI1 cells exhibited reduced mRNA expression of PELI1 (Figure 3D). In addition, the LPS-induced expression of coagulation-related genes *TF* and *PAI-1* was markedly attenuated following *PELI1* silencing (Figure 3E,F). Similarly, the mRNA levels of key inflammatory cytokines, including TNF-α, IL-1β, and IL-6, were significantly decreased in shPELI1 cells upon LPS stimulation (Figure 3G–I). At the protein level, western blot analysis demonstrated coordinated downregulation of PELI1, TF, and PAI-1 proteins in shPELI1 cells following LPS stimulation (Figure 3J). Densitometric analysis further confirmed significant reductions in PELI1, TF, and PAI-1 protein expression compared with control cells (Figure 3K–M). To explore the underlying mechanism, we examined activation of the JAK2/STAT3 signaling pathway. Western blot analysis showed that LPS stimulation markedly increased phosphorylation of JAK2 and STAT3, whereas *PELI1* knockdown substantially suppressed this phosphorylation without affecting total JAK2 or STAT3 levels (Figure 3N). Quantitative analysis confirmed significant reductions in p-JAK2/JAK2 and p-STAT3/STAT3 ratios in shPELI1 cells (Figure 3O,P). Together, these findings indicate that PELI1 promotes inflammation and affects coagulation in macrophages through activation of the JAK2/STAT3 signaling pathway.

PELI1 silencing reduces secretion of inflammatory and coagulation mediators

We next measured secreted protein levels in supernatants from LPS-stimulated macrophages. ELISA results demonstrated that *PELI1* knockdown decreased the release of TF, PAI-1, TNF-α, IL-1β, and IL-6 compared to shNC controls (Figure 4A–E). These results align with intracellular expression data and confirm that PELI1 modulates the secretory profile of macrophages.

PELI1-deficient macrophage secretome ameliorates sepsis: transfer of LPS-stimulated BMDMs conditioned medium recapitulates the knockout phenotype

To determine whether the macrophage secretome mediates the protection afforded by *PELI1* deficiency, we administered CM from LPS-stimulated *Peli1*$^{-/-}$ BMDMs (KOsup) to septic WT mice. Control mice received CM from WT BMDMs (WTsup).

Strikingly, treatment with KOsup—but not WTsup—recapitulated the protective phenotype observed in septic *Peli1*$^{-/-}$ mice. This was evidenced by a comprehensive attenuation of both inflammatory and coagulopathic responses.

As shown in Figure 5A–F, the mRNA expression of PELI1, TF, PAI-1, TNF-α, IL-1β, and IL-6 was reduced in the KOsup-treated group compared with the WTsup-treated group. Consistently, plasma levels of coagulation markers, including TF, D-dimer, and TAT, were decreased in mice receiving KOsup (Figure 5G–I). Western blotting densitometric analyses further demonstrated

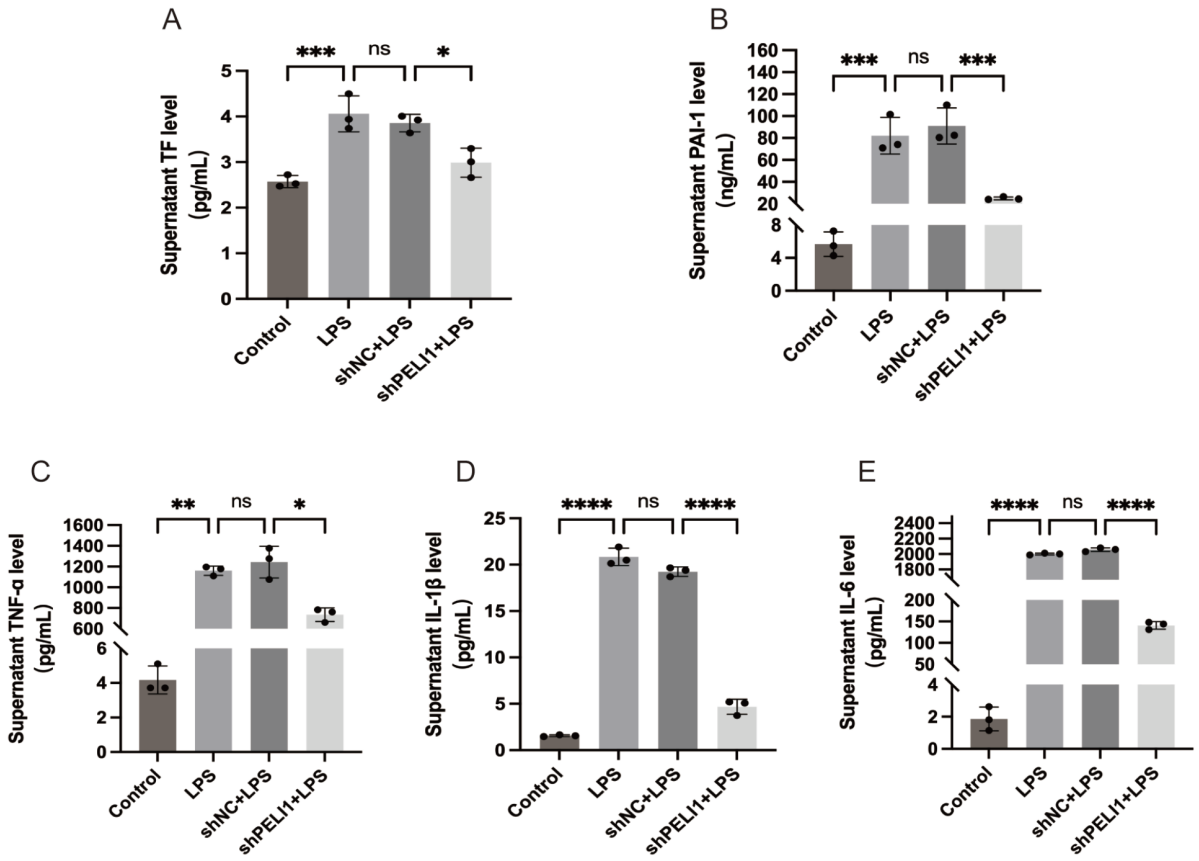


Figure 4. Knockdown of *PELI1* inhibits the secretion of inflammation and coagulation-related factors from macrophages (A–E) Concentrations of (A) TF, (B) PAI-1, (C) TNF-α, (D) IL-1β, and (E) IL-6 in supernatants of RAW264.7 cells, as detected by ELISA. Data are presented as the mean ± SD. Data are representative of three independent experiments. *$P < 0.05$, **$P < 0.01$, ***$P < 0.001$, ****$P < 0.0001$, and ns, $P > 0.05$.

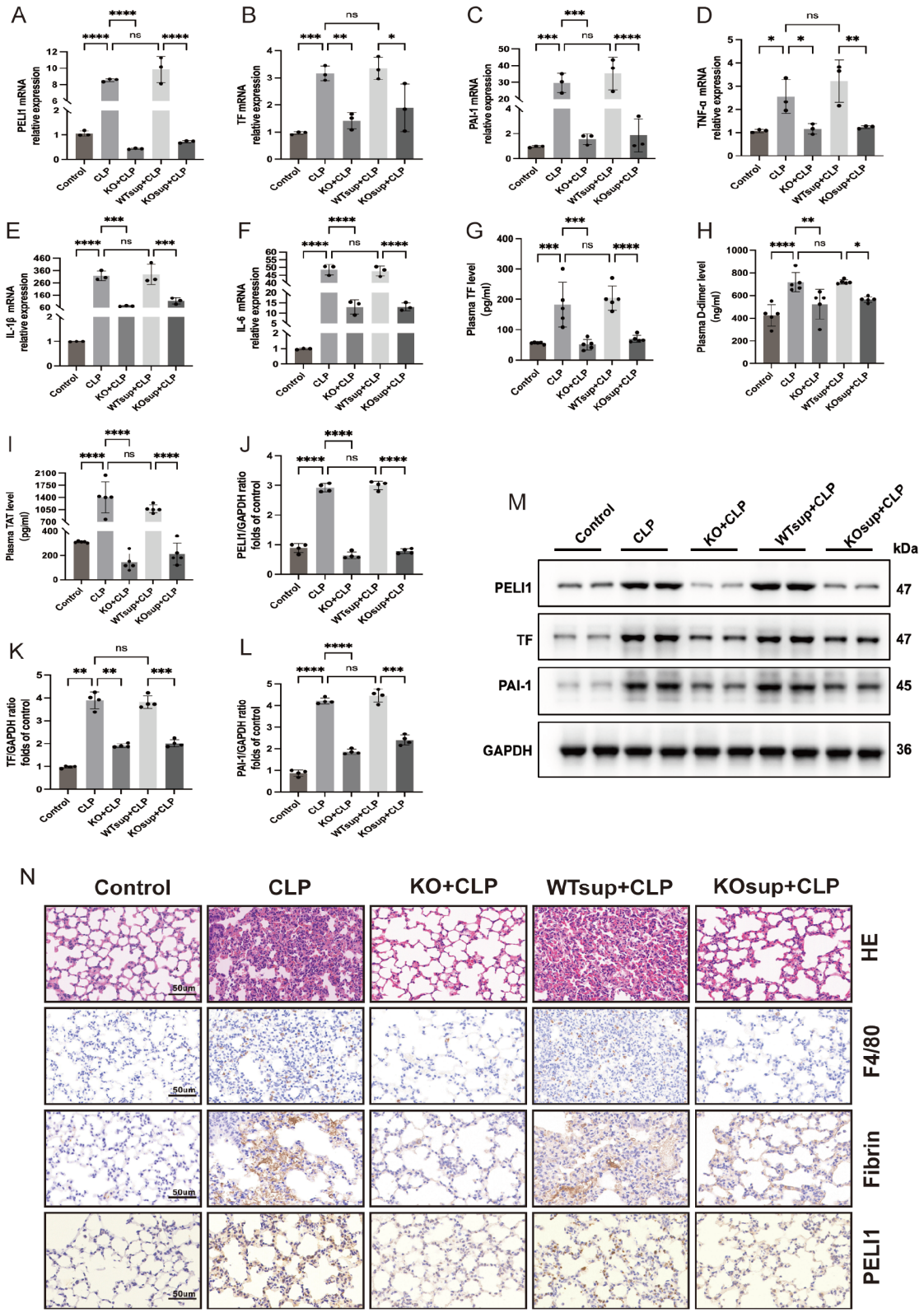


Figure 5. Macrophage *PELI1* deficiency confers sepsis protection potentially via its secretome (A–F) Relative mRNA levels in murine lung tissues: (A) PELI1, (B) TF, (C) PAI-1, (D) TNF-α, (E) IL-1β, and (F) IL-6. (G–I) Plasma levels of coagulation-related markers measured by ELISA: (G) TF, (H) D-dimer, and (I) TAT complex. (J–L) Densitometric analyses of western blot results showing protein expression of (J) PELI1, (K) TF, and (L) PAI-1 in lung tissues. (M) Representative western blot images showing PELI1, TF, and PAI-1 protein expression in lung tissues. (N) Representative lung sections subjected to H&E staining and immunohistochemical staining for F4/80, fibrin, and PELI1 (scale bar: 50 μm). Data are presented as the mean ± SD. *$P < 0.05$, **$P < 0.01$, ***$P < 0.001$, ****$P < 0.0001$, and ns, $P > 0.05$.

significantly reduced protein expression of PELI1 (Figure 5J), TF (Figure 5K), and PAI-1 (Figure 5L) in lung tissues. Representative western blot images are shown in Figure 5M.

Histopathological analysis further validated the protective effects. H&E staining revealed ameliorated lung injury with reduced alveolar wall thickness (Figure 5N). Immunostaining consistently showed diminished infiltration of F4/80$^+$ macrophages, fibrin deposition, and PELI1$^+$ cells in the lungs (Figure 5N). Notably, immunofluorescence co-localization analysis in septic lungs from the original model confirmed that the upregulation of PELI1 occurred predominantly within F4/80$^+$ macrophage infiltrates (Supplementary Figure S3), underscoring the macrophage-centric expression pattern of PELI1 during sepsis.

Collectively, these data demonstrate that the protective effects of *PELI1* deficiency are primarily mediated and can be transferred via the macrophage secretome, effectively mimicking the genetic knockout in ameliorating sepsis-induced lung injury and coagulation dysfunction.

Discussion

Our findings demonstrate that targeting macrophage PELI1 improves septic inflammation and coagulation dysfunction by reprogramming the secretome through the JAK2/STAT3 axis.

We initially identified the specific upregulation of PELI1 in monocytes from septic non-survivors through single-cell transcriptomic analysis, which was subsequently validated at the protein level in FACS-isolated CD14$^+$ monocytes from an independent patient cohort. These findings were corroborated in a murine model, where PELI1 upregulation exacerbated the severity of lung injury and coagulation dysfunction, providing a potential mechanistic explanation for the high mortality rate associated with this molecular endotype [23]. Mechanistically, we found that *PELI1* silencing suppressed LPS-induced phosphorylation of JAK2 and STAT3 without altering their total protein levels, consequently reducing the expression of key inflammatory cytokines (TNF-α, IL-6, IL-1β) and coagulation factors (TF, PAI-1). Although prior studies have suggested STAT3 as a downstream target of PELI1 [20], our data demonstrate for the first time that *PELI1* knockdown functionally suppresses the activation of the JAK2/STAT3 pathway in sepsis, identifying it as a central regulatory hub coordinating both inflammatory and coagulatory responses. Direct validation of the PELI1-STAT3 molecular interaction in this context remains a key objective for future investigation. Inspired by the therapeutic potential of cell-derived products, such as mesenchymal stem cell-conditioned medium [24–31], we hypothesized that the protection conferred by PELI1 deficiency might stem from an altered secretome. Experiments confirmed that *PELI1* knockdown in macrophages significantly reduced the secretion of inflammatory factors and coagulation mediators. More importantly, adoptive transfer of conditioned medium from *Peli1*$^{-/-}$ macrophages into septic wild-type mice was sufficient to recapitulate the protective phenotype observed in genetic knockout models, effectively alleviating systemic coagulation dysfunction and lung tissue injury. This discovery not only reinforces the concept of "cell-specific secretome regulation" [32], but also establishes the secretome from *PELI1*-deficient macrophages itself as a promising "cell-free" therapeutic strategy.

In summary, by integrating clinical data with animal models, this study systematically elucidates the central role of macrophage PELI1 in sepsis and unveils a novel mechanism whereby modulation of the PELI1-JAK2/STAT3 axis contributes to pathology by reprogramming the macrophage secretome. This suggests a potential dual therapeutic strategy for sepsis: first, targeting PELI1 as a candidate for intervention and, second, directly utilizing the protective components within the *PELI1*-deficient secretome as a basis for novel therapeutic agents.

This study has several limitations. First, the use of a global *Peli1* knockout model, while strongly supported by secretome transfer and co-localization data, does not entirely exclude potential minor contributions from other immune cell types. Second, the direct molecular interaction between PELI1 and STAT3 in the context of sepsis was not validated here and awaits confirmation in future studies. Third, our mechanistic investigation focused on a defined panel of macrophage-centric coagulation markers (TF, PAI-1) and systemic indicators (TAT, D-dimer). Although this panel effectively captures axis-specific procoagulant activity, a comprehensive clinical coagulation profile [33] will be important in future work to fully assess the translational relevance of our findings. Finally, the key protective constituents within the *Peli1*$^{-/-}$ macrophage secretome and their direct *in vivo* targets remain to be identified, which represents a primary goal for our next phase of research.

In summary, this study establishes the pivotal role of macrophage PELI1 and its regulated secretome in septic inflammation and coagulation dysfunction. Targeting the PELI1-JAK2/STAT3 signaling axis or utilizing the *PELI1*-deficient secretome represents a highly promising therapeutic strategy.

Supplementary Data

Supplementary data are available at *Acta Biochimica et Biophysica Sinica* online.

Data Availability

The raw sequencing data have been deposited in the NCBI BioProject database under accession number PRJNA1359544. Data can be accessed upon reasonable request from the corresponding author.

Acknowledgement

We sincerely thank all those who devoted much time to reading this thesis and gave us much advice. We thank Dr Xindong Cai from the laboratory of Professor Jinsong Li at the Center for Excellence in Molecular Cell Science, Chinese Academy of Sciences, for generously providing the *Peli1*-knockout mice.

Funding

This work was supported by the grants from the Innovation Fund of Zhongshan Hospital, Fudan University (No. 2023-2ZSCX12), the Shanghai Public Health Talent Development Program for Outstanding Discipline Leaders (No. GWVI-11.2-XD36), the Shanghai Science and Technology Commission (No. 20S31905300), and the Chinese Medical Association Medical Education Research Project (No. 2025B54).

Conflict of Interest

The authors declare that they have no conflict of interest.

References

1. Gassmann B. Speaking with one voice. *Krankenpfl Soins Infirm* 2002, 95: 7

2. Vincent JL, Opal SM, Marshall JC, Tracey KJ. Sepsis definitions: time for change. *Lancet* 2013, 381: 774–775
3. Rudd KE, Johnson SC, Agesa KM, Shackelford KA, Tsoi D, Kievlan DR, Colombara DV, *et al.* Global, regional, and national sepsis incidence and mortality, 1990–2017: analysis for the global burden of disease study. *Lancet* 2020, 395: 200–211
4. Reddy H, Javvaji CK, Malali S, Kumar S, Acharya S, Toshniwal S. Navigating the cytokine storm: a comprehensive review of chemokines and cytokines in sepsis. *Cureus* 2024, 16: e54275
5. Cavaillon JM, Adib-Conquy M. Monocytes/macrophages and sepsis. *Crit Care Med* 2005, 33: S506–S509
6. Rothmeier AS, Marchese P, Petrich BG, Furlan-Freguia C, Ginsberg MH, Ruggeri ZM, Ruf W. Caspase-1-mediated pathway promotes generation of thromboinflammatory microparticles. *J Clin Invest* 2015, 125: 1471–1484
7. Rosseau S, Hammerl P, Maus U, Walmrath HD, Schütte H, Grimminger F, Seeger W, *et al.* Phenotypic characterization of alveolar monocyte recruitment in acute respiratory distress syndrome. *Am J Physiol-Lung Cell Mol Physiol* 2000, 279: L25–L35
8. Xia W, Mao Y, Xia Z, Cheng J, Jiang P. RETRACTED ARTICLE: metabolic remodelling produces fumarate via the aspartate-argininosuccinate shunt in macrophages as an antiviral defence. *Nat Microbiol* 2025, 10: 1115–1129
9. Kim JY, Cho DW, Choi JY, Jeong S, Kang M, Kim WJ, Hong IS, *et al.* CXCL11 reprograms M2-biased macrophage polarization to alleviate pulmonary fibrosis in mice. *Cell Biosci* 2024, 14: 140
10. Sachetto ATA, Mackman N. Monocyte tissue factor expression: lipopolysaccharide induction and roles in pathological activation of coagulation. *Thromb Haemost* 2023, 123: 1017–1033
11. Wu C, Lu W, Zhang Y, Zhang G, Shi X, Hisada Y, Grover SP, *et al.* Inflammasome activation triggers blood clotting and host death through pyroptosis. *Immunity* 2019, 50: 1401–1411.e4
12. Grover SP, Mackman N. Tissue factor. *Arterioscler Thromb Vasc Biol* 2018, 38: 709–725
13. Pawlinski R, Wang JG, Owens Iii AP, Williams J, Antoniak S, Tencati M, Luther T, *et al.* Hematopoietic and nonhematopoietic cell tissue factor activates the coagulation cascade in endotoxemic mice. *Blood* 2010, 116: 806–814
14. Levi M, Scully M. How I treat disseminated intravascular coagulation. *Blood* 2018, 131: 845–854
15. Mackman N, Tilley RE, Key NS. Role of the extrinsic pathway of blood coagulation in hemostasis and thrombosis. *Arterioscler Thromb Vasc Biol* 2007, 27: 1687–1693
16. Chang M, Jin W, Sun SC. Peli1 facilitates TRIF-dependent Toll-like receptor signaling and proinflammatory cytokine production. *Nat Immunol* 2009, 10: 1089–1095
17. Chen H, Hou Y, Zhai Y, Yang J, Que L, Liu J, Lu L, *et al.* Peli1 deletion in macrophages attenuates myocardial ischemia/reperfusion injury by suppressing M1 polarization. *J Leukoc Biol* 2023, 113: 95–108
18. Lin D, Hu L, Wei D, Li Y, Yu Y, Wang Q, Sun X, *et al.* Peli1 deficiency in macrophages attenuates pulmonary hypertension by enhancing foxp1-mediated transcriptional inhibition of IL-6. *Hypertension* 2025, 82: 445–459
19. Hu BC, Wu GH, Shao ZQ, Zheng Y, Liu JQ, Zhang R, Hong J, *et al.* Redox DAPK1 destabilizes Pellino1 to govern inflammation-coupling tubular damage during septic AKI. *Theranostics* 2020, 10: 11479–11496
20. Hwang S, Park J, Koo SY, Lee SY, Jo Y, Ryu D, Go H, *et al.* The ubiquitin ligase Pellino1 targets STAT3 to regulate macrophage-mediated inflammation and tumor development. *Nat Commun* 2025, 16: 1256
21. Beckman JD, DaSilva A, Aronovich E, Nguyen A, Nguyen J, Hargis G, Reynolds D, *et al.* JAK-STAT inhibition reduces endothelial prothrombotic activation and leukocyte-endothelial proadhesive interactions. *J Thromb Haemost* 2023, 21: 1366–1380
22. Buka RJ, Montague SJ, Moran LA, Martin EM, Slater A, Watson SP, Nicolson PLR. PF4 activates the c-Mpl-Jak2 pathway in platelets. *Blood* 2024, 143: 64–69
23. Mekata K, Kyo M, Tan M, Shime N, Hirohashi N. Molecular endotypes in sepsis: integration of multicohort transcriptomics based on RNA sequencing. *J Intensive Care* 2025, 13: 30
24. Hou X, Zhang X, Zhao W, Zeng C, Deng B, McComb DW, Du S, *et al.* Vitamin lipid nanoparticles enable adoptive macrophage transfer for the treatment of multidrug-resistant bacterial sepsis. *Nat Nanotechnol* 2020, 15: 41–46
25. Sloas C, Gill S, Klichinsky M. Engineered CAR-macrophages as adoptive immunotherapies for solid tumors. *Front Immunol* 2021, 12: 783305
26. Liu X, Xu W, Feng J, Wang Y, Li K, Chen Y, Wang W, *et al.* Adoptive cell transfer of piezo-activated macrophage rescues immunosuppressed rodents from life-threating bacterial infections. *Nat Commun* 2025, 16: 1363
27. Deng Y, Chen Q, Yang X, Sun Y, Zhang B, Wei W, Deng S, *et al.* Tumor cell senescence-induced macrophage CD73 expression is a critical metabolic immune checkpoint in the aging tumor microenvironment. *Theranostics* 2024, 14: 1224–1240
28. Rostami J, Mothes T, Kolahdouzan M, Eriksson O, Moslem M, Bergström J, Ingelsson M, *et al.* Crosstalk between astrocytes and microglia results in increased degradation of α-synuclein and amyloid-β aggregates. *J Neuroinflamm* 2021, 18: 124
29. Sendon-lago J, Seoane S, Saleh F, Garcia-caballero L, Arias ME, Eiro N, Macia M, *et al.* *In vivo* effects of conditioned medium from human uterine cervical stem cells in an ovarian cancer xenograft mouse model. *Cancer Genomics Proteomics* 2022, 19: 570–575
30. Nuzzo AM, Moretti L, Mele P, Todros T, Eva C, Rolfo A. Effect of placenta-derived mesenchymal stromal cells conditioned media on an LPS-induced mouse model of preeclampsia. *Int J Mol Sci* 2022, 23: 1674
31. Xue R, Xie M, Wu Z, Wang S, Zhang Y, Han Z, Li C, *et al.* Mesenchymal stem cell-derived exosomes promote recovery of the facial nerve injury through regulating macrophage M1 and M2 polarization by targeting the P38 MAPK/NF-Kb pathway. *Aging Dis* 2024, 15: 851–868
32. Mehrotra P, Maschalidi S, Boeckaerts L, Maueröder C, Tixeira R, Pinney J, Burgoa Cardás J, *et al.* Oxylipins and metabolites from pyroptotic cells act as promoters of tissue repair. *Nature* 2024, 631: 207–215
33. Zhang J, Zhu X, Li Y, Wu Y, Du Y, Yang H, Liu Z, *et al.* Parthenolide improves sepsis-induced coagulopathy by inhibiting mitochondrial-mediated apoptosis in vascular endothelial cells through BRD4/BCL-xL pathway. *J Transl Med* 2025, 23: 80